Parkinson's disease–associated VPS35 mutant reduces mitochondrial membrane potential and impairs PINK1/Parkin-mediated mitophagy

Kai Yu Ma
University Medical Center Groningen https://orcid.org/0000-0001-6300-0882
Michiel R Fokkens
University Medical Center Groningen
Fulvio Reggiori
University Medical Center Groningen
Muriel Mari
University Medical Center Groningen
Dineke S Verbeek (d.s.verbeek@umcg.nl)
University Medical Center Groningen https://orcid.org/0000-0002-4759-7006

Research article

Keywords: VPS35, PINK1, Parkin, pathogenesis

Posted Date: December 22nd, 2020

DOI: https://doi.org/10.21203/rs.3.rs-131693/v1

Abstract

Background:

Mitochondrial dysfunction plays a prominent role in the pathogenesis of Parkinson's disease (PD), and several genes linked to familial PD, including *PINK1* and *PARK2*, are directly involved in processes such as mitophagy that maintain mitochondrial health. The dominant p.D620N variant in *VPS35* has also been associated to familial PD but has not been functionally connected to *PINK1* and *PARK2*.

Methods:

To better mimic and study the patient situation, we used CRISPR-Cas9 to generate heterozygous human SH-SY5Y cells carrying the PD-associated D620N variant in *VPS35*. These cells were treated with the protonophore CCCP to induce PINK1/Parkin-mediated mitophagy, which was assessed using biochemical and microscopy approaches.

Results:

Mitochondria in VPS35-D620N cells exhibited reduced mitochondrial membrane potential and appeared to already be damaged at steady state. As a result, the mitochondria of these cells were desensitized to CCCP-induced collapse in mitochondrial potential, as they displayed altered fragmentation and were unable to accumulate PINK1 at their surface upon this insult. Consequently, Parkin recruitment to the cell surface was inhibited and initiation of PINK1/Parkin-dependent mitophagy is impaired.

Conclusion:

Our findings extend the pool of evidence that the p.D620N mutant VPS35 causes mitochondrial dysfunction and suggest a converging pathogenic mechanism between VPS35, PINK1 and Parkin in PD.

Background

Parkinson's disease (PD) is the second most common age-related neurodegenerative disorder, affecting more than 10 million people worldwide[1]. Most patients develop the disease in a sporadic manner through a complex interaction between genetic and environmental risk factors while ageing. Roughly 5–10% of PD is caused by highly penetrant variants in genes such as *PINK1* and *PARK2*[2,3]. This type of PD is referred to as familial PD, and missense variants in *VPS35* have been linked to the autosomal dominant form of familial PD[4,5]. However, the c.1858G > A, pD620N variant in *VPS35* is the only proven pathogenic variant[6]. *VPS35* encodes the vacuolar protein sorting-associated protein 35 (VPS35) that, together with VPS26 and VPS29, forms the cargo-selective subcomplex of the retromer complex[7]. Retromer recycles membrane proteins from endosomes to either the Golgi apparatus or the plasma membrane[8]. The p.D620N variant is located in a domain of VPS35 that is essential for protein–protein interactions[7]. Although the variant does not affect the formation of the retromer complex, it impairs its interactions with

other factors such as actin-nucleating Wiskott-Aldrich syndrome and SCAR homolog (WASH) complex[9,10]. This leads to altered retromer functioning and deficits in the sorting of cargos[9–12].

Retromer also participates in the transport of mitochondrial cargos to lysosomes or peroxisomes via mitochondrial-derived vesicles (MDVs)[13–15]. Previous reports have shown that VPS35 is involved in mitochondrial dynamics, as it recycles the fission protein DLP1 and regulates levels of the fusion protein MFN2 through the transport of mitochondrial E3 ubiquitin ligase 1 (MUL1)[14,15]. Overexpression of D620N-mutant VPS35 augments mitochondrial fragmentation due to increased DLP1 activity, whereas VPS35 depletion leads to mitochondrial fragmentation as result of decreased levels of MFN2, which correlates with reduced mitochondrial respiratory capacity and a decrease in mitochondrial membrane potential[14–16].

Mitochondrial dysfunction plays an integral role in the pathogenesis of both sporadic and familial PD[17–19]. For example, loss-of-function variants in mitochondrial quality control genes such as *PINK1* (encoding PTEN-induced putative kinase 1 (PINK1)) and *PARK2* (encoding the E3 ubiquitin ligase Parkin) led to early-onset autosomal recessive PD[2,3,20–22]. To maintain mitochondrial quality, PINK1 is imported through a membrane potential–dependent process, from the outer mitochondrial membrane (OMM) into the inner mitochondrial membrane, where it is constitutively degraded by mitochondrial proteases[23,24]. However, PINK1 import and cleavage is blocked upon mitochondrial depolarization caused by damage, resulting in the accumulation of PINK1 on the OMM. At the OMM, PINK1 phosphorylates ubiquitin and Parkin, leading to stable recruitment and activation of Parkin onto the mitochondrial surface[21,24,25]. Parkin then ubiquitinates different OMM substrates, inducing proteasomal degradation and removal of damaged cargos via MDVs-to-lysosome transport and/or mitophagy[26–28].

Mitophagy is a selective type of autophagy in which mitochondria targeted for degradation are sequestered into double-membrane autophagosomes and delivered into lysosomes[29,30]. This process occurs in different physiological contexts[30]. For instance, most cells continuously undergo basal mitophagy during routine mitochondrial maintenance[31]. However, mitophagy can also be induced as a response to mitochondrial stressors such as mitochondrial depolarization. Notably, the PD-associated proteins PINK1 and Parkin are directly involved in stress-induced mitophagy[21,24] but not in basal mitophagy[32,33]. As dopaminergic neurons undergo substantial mitochondrial stress, presumably due to their pacemaker activity[34,35], stress-induced mitophagy via PINK1/Parkin has been heavily implicated in the pathogenesis of PD[30].

Given the mitochondrial impairments associated with the p.D620N variant in *VPS35* and the role of PINK1 and Parkin in maintaining mitochondrial quality control under stress conditions, we questioned whether the actions of these genes converge into a similar pathway to cause PD. Therefore, we set out to determine whether stress-induced mitophagy via PINK1/Parkin is affected by p.D620N-mutant VPS35. In the present study, we generated mutant VPS35 SH-SY5Y cells that carry the p.D620N variant on one allele, recapitulating the patient situation. We show that these cells are unable to accumulate PINK1 when

treated with carbonyl cyanide m-chlorophenylhydrazone (CCCP) and subsequently fail to recruit Parkin to mitochondria. The mitochondria of D620N-mutant VPS35 cells exhibit reduced mitochondrial membrane potential and appear already damaged under steady state conditions. The D620N-mutant VPS35 cells are likely desensitized to CCCP-induced mitochondrial damage, resulting in impairments in PINK1/Parkin-mediated mitophagy. Together, these data advocate for convergent pathways in PD and link VPS35 to PINK1 and Parkin.

Materials And Methods

Cell culture, transient transfections and treatments

Human SH-SY5Y neuroblastoma cells were maintained in Dulbecco's Modified Eagle's Medium (Invitrogen) supplemented with 15% fetal bovine serum (Invitrogen) and 1% Penicillin-Streptomycin (Gibco) in a 37°C incubator with 5% CO_2. Transient plasmid transfections were performed with plasmid DNAs using Lipofectamine (Thermo), according to the manufacturer's instructions. To induce mitochondrial depolarization, SH-SY5Y cells were treated with either 10 μM or 20 μM CCCP (Sigma-Aldrich), 1 μM oligomycin (Sigma-Aldrich), 1 μM antimycin A (Sigma-Aldrich) or 1 μM antimycin A and 1 μM oligomycin for the indicated times, prior to cell harvesting or fixation. DMSO was used as a control treatment.

Expression plasmids and antibodies

The plasmids used were pEGFP-Parkin[36] (a gift from Edward Fon, Addgene plasmid #45875) and pEGFP-LC3 (a gift from Toren Finkel, Addgene plasmid #24920) constructs[37]. The primary antibodies used for immunoblotting were mouse anti-β-Actin (1:5000, MP Biomedicals 8691001), mouse anti-β-Tubulin (1:5000, Sigma T4026), rabbit anti-COXIV (1:1000, Proteintech 11242-1-AP), mouse anti-Parkin (1:500, Santa-Cruz Biotechnology sc-32282), rabbit anti-PINK1 (1:1000, Cell signaling #6946), mouse anti-SQSTM1/p62 (1:500, Santa Cruz Biotechnology sc-28359), mouse anti-TOM20 (1:500, BD Biosciences 612278) and goat anti-VPS35 (1:1000, Abcam ab10099). The primary antibodies used for immunofluorescence (IF) were mouse anti-TOM20 (1:200, Santa Cruz Biotechnology sc-17764) and rabbit anti-PINK1 (1:200, Abcam ab216144). Secondary antibodies for immunoblotting were HRP-conjugated goat anti-rabbit IgG (H+L) (1:10,000, Bio-Rad), HRP-conjugated goat anti-mouse IgG (H+L) (1:10,000, Bio-Rad) and HRP-conjugated donkey anti-goat IgG (H+L) (1:10,000, Abcam). Secondary antibodies for IF were Cy3-conjugated donkey anti-mouse IgG (H+L) (1:250, Jackson ImmunoResearch) and Alexa Fluor 488-conjugated donkey anti-rabbit IgG (H+L) (1:250, Jackson ImmunoResearch).

Generation of VPS35 D620N/WT SH-SY5Y cells

The D620N mutation in the *VPS35* gene was obtained by Clustered Regularly Interspaced Short Palindromic Repeats (CRISPR)-Cas9—mediated genome editing in the SH-SY5Y neuroblastoma cell line, as previously described[38]. Briefly, a 20-nt sgRNA sequence that targets exon 15 of the *VPS35* gene and is predicted to cut approximately 9 base-pairs (bp) upstream of the GAT triplet encoding the aspartic acid

residue on location 620 was cloned into the pSpCas9(BB)-2A-GFP (PX458) plasmid (a gift from Feng Zhang, Addgene plasmid #48138) using the BbsI restriction enzyme to form the targeting plasmid expressing Cas9-GFP. In addition, a single-stranded oligodeoxynucleotide sequence was designed to facilitate homology-directed repair of the endogenous locus and included the substitution of five nucleotides: a nucleotide substitution G>A that leads to the D620N mutation in *VPS35* and four synonymous substitutions that create a novel *EcoRI* restriction site that also destroys the protospacer-adjacent motif sequence to avoid repetitive cutting of Cas9 by the repair template. Following validation, the PX458-sgRNA plasmid and the single-stranded oligonucleotides were transfected into SH-SY5Y cells, following the manufacturer's protocol (Lonza). GFP-positive cells were single-cell sorted 48 hours post-transfection using a SH800S cell sorter (Sony Biotechnology) and grown in separate cultures that were subsequently screened for the D620N mutation using the restriction enzyme *EcoRI*. In parallel, we mock-electroporated and sorted the same batch of cells, which were used as wild type (WT) control in the following experiments. Finally, we sequenced the top three predicted off-target genomic regions within coding regions (obtained from http://crispr.mit.edu) in the genes *POU6F1, ZNF318* and *KY* but found no off-target edits (not shown). Detailed primer and template sequences are provided in Supplementary Table 1.

Generation of stable COX8-EGFP-mCherry reporter SH-SY5Y cells

The COX8-EGFP-mCherry sequence was obtained from the pCLBW COX8-EGFP-mCherry construct[39] (a gift from David Chan, Addgene plasmid #78520) through restriction enzyme digestion with *ApaI* and *EcoRI* and was ligated into the mammalian expression vector pcDNA 3.1(+). Subsequently, the vector was transfected into WT and VPS35^{D620N} SH-SY5Y cells using Lipofectamine 3000 (Thermo Scientific), following the manufacturer's protocol. 48 hours after transfection, the growth medium was replaced with selection medium containing 800 ng/µl G-418 (Sigma-Aldrich). The selection medium was refreshed every other day for 10 days, until only cells with the plasmid remained. Stable cell lines were cultured for three passages before performing the experiments.

Protein extraction and immunoblotting

SH-SY5Y cells were harvested in 2% sodium dodecyl sulfate (SDS)/phosphate-buffered saline (PBS) buffer containing a proteinase inhibitor cocktail (Roche) and sonicated. Crude mitochondrial fractions were isolated, as previously described[40]. Briefly, SH-SY5Y cells were collected and cracked using a Dounce homogenizer in ice cold isolation buffer containing 320 mM sucrose and proteinase inhibitor cocktail. Homogenized samples were differentially centrifuged at 1500g for 15 min and 17,000g for 30 min to obtain nuclei and crude mitochondria, respectively. The cytosolic fraction was obtained from the final supernatant. Protein concentrations were quantified using the Pierce™ BCA protein assay kit (Thermo Scientific), and samples were mixed with loading sample buffer containing 10% β-mercaptoethanol before being boiled at 95°C for 5 min. Subsequently, equal amounts of total protein extracts were subjected to SDS-PAGE, transferred to nitrocellulose membranes, blocked for 1 h in skimmed milk and incubated overnight with primary antibody at 4°C and then with the corresponding

secondary antibody for 1 h at room temperature (RT). Blots were imaged on a Chemidoc™ MP Imaging System (Bio Rad). Protein levels were quantified using densitometry in ImageJ software (NIH).

Immunofluorescence

WT and VPS35^{D620N} SH-SY5Y cells that were seeded on glass coverslips in 24-well plates were fixed in 4% paraformaldehyde in PBS for 10 min at RT. Cells were then permeabilized in 0.1% Triton X-100 in PBS for 10 min and blocked with 5% donkey serum (Abcam) in PBS for 1 h. Coverslips were then incubated overnight at 4°C with the primary antibodies diluted in blocking buffer and for 1 h at RT for secondary antibody incubation. Coverslips were finally mounted onto glass slides in 4',6-diamidino-2-phenylindole (DAPI)-containing mounting medium (Vectashield). The slides were analyzed using either structured illumination microscopy (SIM) or confocal microscopy. SIM images were acquired with an AxioObserver Z1 compound microscope (Carl Zeiss) equipped with an Apotome, 63x oil objective and an AxioCam MRm3 CCD camera (Carl Zeiss). Confocal images were acquired with a TCS SP8 high-resolution confocal laser scan microscope (Leica) and an HC PL APO CS2 63x/1,4 oil objective. For quantitative analysis, maximum intensity projections were generated from all Z-stacks, which were captured for each condition with identical exposure times or laser settings.

Image analysis

All image analyses were performed using ImageJ software (NIH). Colocalization analyses of PINK1 and TOM20 were performed using ImageJ plugin Coloc 2 (https://imagej.net/Coloc_2). Regions of interest (ROIs) were created per cell in the TOM20 channel (n = ~ 80–100 cells per condition in each experiment). Pearson's correlation coefficients were subsequently determined per ROI using the Costes method for threshold regression[41].

Mitochondrial morphology was quantified as previously described[42]. Briefly, images of single cells were pre-processed and binarized, followed by particle analysis and computation of several metrics. The number of mitochondria was determined as the number of individual particles. The aspect ratio was determined by dividing the major axis by the minor axis of each particle. A total of 80–100 cells were quantified per condition in each experiment.

For the EGFP-Parkin translocation experiment, a blinded observer scored each cell for either diffuse EGFP-Parkin or mitochondria-localized EGFP-Parkin (n = ~50 cells per condition in each experiment), as previously described[36].

Mitophagy using COX8-EGFP-mCherry stable cell lines was quantified by determining the ratio of the number of particles obtained from the mCherry channel (mitophagolysosomes) and the number of particles obtained from the EGFP channel (mitochondria) per cell (n= ~50–70 cells per condition in each experiment). Particles were analyzed in a similar fashion to the mitochondrial morphology quantification.

EGFP-LC3 puncta on mitochondria were quantified as follows: a mask was created from the TOM20 mitochondrial staining and used as overlay over the EGFP-LC3 image. Puncta were subsequently counted for each cell (n = ~40–50 cells per experiment).

Mitochondrial membrane potential quantification

Mitochondrial membrane potential was measured using fluorescence-activated cell sorting (FACS). WT and VPS35^{D620N} SH-SY5Y cells were incubated for 30 min with 100 nM tetramethylrhodamine methyl ester (TMRM) dye (Thermo Scientific) and 100 nM MitoTracker Green FM dye (Thermo Scientific) diluted in culture medium. Cells were rinsed, dissociated with 0.05% Trypsin-EDTA (Thermo) and aliquoted in multiple FACS tubes. FACS measurements were performed with a FACSCalibur flow cytometer (BD Biosciences). After baseline measurements, CCCP was added to a final concentration of 10 µM, upon which measurements were taken at each time point. Three independent sorts measuring at least 10,000 cells were performed per clone per time point. Data analysis was performed using Kaluza Analysis software (Beckman Coulter). Mitotracker Green median fluorescence intensity was used to correct for mitochondrial mass fluctuations.

Ultrastructural analyses

For conventional transmission electron microscopy (TEM), WT and VPS35^{D620N} SH-SY5Y cells were treated with DMSO or 10 µM CCCP for 6 h. An equal volume as the culture media of double-strength fixative (4% paraformaldehyde, 5% glutaraldehyde in 0.1 M sodium cacodylate buffer, pH 7.4) was then added to the cells for 20 min at RT, prior to further fixing the cells with one volume of single-strength fixative (2% paraformaldehyde, 2.5% glutaraldehyde in 0.1 M sodium cacodylate buffer, pH 7.4) for 2 h at RT. After five washes with 0.1 M sodium cacodylate buffer (pH 7.4), cells were scraped and embedded, as previously described[43]. Subsequently, 70 nm ultrathin sections were cut using a Leica EM UC7 ultra microtome (Leica Microsystems) and stained with uranyl acetate and lead citrate, as previously described[43]. Cell sections were analyzed using an 80 kV transmission electron microscope CM100bio TEM (FEI).

The analysis of the different mitochondria profiles per cell type was performed by random screening of sections derived from at least three different grids per sample. The mitochondria profiles were categorized as follows: classical mitochondria with well-defined cristae (category I), dark mitochondria with well-defined cristae often swelling (category II), mitochondria with undefined cristae (category III), dark mitochondria with undefined contours and cristae (category IV) and large mitochondria with very light content and few remnant cristae (category V). The number of each mitochondrial type per condition was determined by counting 665, 579 and 521 mitochondria profiles from DMSO-treated WT and VPS35^{D620N} cell (clone 1 and 2) sections, respectively, and 727, 1028 and 914 mitochondria profiles from CCCP-treated WT and VPS35^{D620N} cell (clone 1 and 2) cell sections, respectively.

Cell viability assay

Cell viability upon treatment with CCCP or antimycin A with oligomycin (AO) was determined using a 3-(4,5-demethylthiazol-2-yl)-2,5-diphenyltetrazolium bromide (MTT) reduction assay (Abcam). SH-SY5Y cells were plated in 96-well plates 12 h prior to incubations with CCCP or AO for 24 h. MTT assay compounds were added following the manufacturer's protocol and absorbance was measured using a Synergy HT optical plate reader (Biotek).

Statistical analyses

The data obtained from the Western blot densitometry measurement experiments, mitochondrial membrane potential measurements, TEM and mitochondrial morphology were analyzed using a linear model by one-way or two-way analysis of variance (ANOVA) followed by Tukey's post-hoc test. Count data, such as the EGFP-LC3 and mitochondrial particles quantification, were modelled using a generalized linear model followed by one-way or two-way ANOVA and Tukey's post-hoc test. PINK1-TOM20 colocalization experiments were analyzed using the Kruskal-Wallis test followed by pairwise Mann-Whitney U-test with Benjamini-Hochberg multiple testing correction. Proportional data from the COX8-EGFP-mCherry mitophagy and EGFP-Parkin localization were analyzed using beta regression analysis. Data are means ± standard error of the mean from at least three independent experiments, unless otherwise specified. A p-value < 0.05 was considered statistically significant. Statistical analyses were computed in R (version 1.3.959).

Results

Generation of heterozygous D620N-mutant VPS35 SH-SY5Y cells

To date, most studies have investigated the p.D620N variant in *VPS35* (VPS35^{D620N}) using stable overexpression of VPS35^{D620N} *in vitro* and *in vivo* models. However, the enhanced VPS35 levels in these models may affect retromer functioning as higher or lower levels of VPS35 are shown to correlate with alterations in mitochondrial fragmentation[14,15]. This motivated us to use CRISPR-Cas9–mediated genome editing to introduce the p.D620N variant in *VPS35* into the human neuroblastoma SH-SY5Y cells widely used in PD research[38,44] (Figure 1A). Restriction fragment length polymorphism analysis using the *EcoRI* enzyme on a 604-bp genomic DNA region surrounding the variant revealed two putative positive clones (Figure 1B). Sanger sequencing validated the presence of the p.D620N variant, created with a GAT to AAT codon change, in only one of two *VPS35* alleles, mimicking the heterozygous carrier status seen in patients (Figure 1C). Additionally, immunoblotting showed that the introduction of the p.D620N variant did not affect the expression levels of VPS35 compared to WT cells (Figure 1D). These cell lines were used for the rest of this study.

PINK1-mediated Parkin recruitment to mitochondria is impaired in CCCP-treated VPS35^{D620N} cells

To investigate whether the p.D620N variant in VPS35 affects PINK1/Parkin-mediated mitophagy, we used the protonophore CCCP to induce mitochondrial stress by dissipating the mitochondrial membrane potential ($\Delta\psi_m$) and thereby activate PINK1/Parkin-mediated mitophagy[21,24,25]. We used immunoblotting to investigate PINK1 accumulation over time in WT and VPS35^{D620N} cells upon 10 μM CCCP treatment. As expected, total PINK1 levels increased slightly after 3 hours of CCCP treatment, and PINK1 accumulation was pronounced after 24 hours of CCCP treatment in whole cell extracts and crude mitochondrial fractions of WT cells (Figure 2A, B). This coincided with a decrease in total Parkin levels (Figure 2A, B), likely due to autoubiquitination and increased proteasomal turnover of mitochondrial-bound Parkin[45]. Total PINK1 levels, however, were substantially lower in the whole extracts and crude mitochondrial fractions of CCCP-treated VPS35^{D620N} cells at both time points compared to WT cells (Figure 2A–D). Likewise, total Parkin levels remained similar to those in the untreated condition (Figure 2A, B). Of note, VPS35 levels did not change upon CCCP treatment (Figure 2A, B), and VPS35 was present in the crude mitochondrial fraction (Figure 2B), in line with previous reports[14,15].

Previous studies have shown a dose-dependent effect of CCCP and thus we questioned whether a higher dose of CCCP would be able to stabilize PINK1 on mitochondria in the VPS35^{D620N} cells. Indeed, 20 μM CCCP led to higher PINK1 levels compared to 10 μM CCCP in WT cells after 24 hours of treatment and marked PINK1 accumulation was now also seen in the VPS35^{D620N} cells (Figure 2C). However, total PINK1 levels in VPS35^{D620N} cells remained significantly lower than those in WT cells (Figure 2C, E). Consistent with the increase in PINK1 levels upon treatment with 20 μM CCCP, proteasomal degradation of Parkin in WT cells also further increased with 20 μM CCCP, which was not observed in VPS35^{D620N} cells (Supplementary figure 1A, B). Of note, 20 μM CCCP demonstrated increased cytotoxicity compared to 10 μM CCCP (Supplementary figure 1C). This data suggests that 10 μM CCCP induces milder damage to mitochondria then 20 μM CCCP and exposes a not-yet-characterized deficit in the VPS35^{D620N} clones.

Next, we used IF to quantify the translocation of cytosolic EGFP-Parkin to mitochondria upon treatment with CCCP, since endogenous Parkin was not detectable in our cells. WT and VPS35^{D620N} cells were transiently transfected with EGFP-Parkin and subsequently treated with 10 μM CCCP for 6 hours and stained for OMM protein TOM20. As expected, mitochondrial depolarization due to CCCP caused translocation of cytosolic EGFP-Parkin to mitochondria in WT cells, as shown by the colocalization between EGFP-Parkin and TOM20 (Figure 2F). Additionally, less Parkin translocation was seen in VPS35^{D620N} cells (± 23% and ±25%) compared to WT cells (± 63%) (Figure 2G). To complement this observation, the colocalization between endogenous PINK1 and TOM20 was determined using IF in WT and VPS35^{D620N} cells upon CCCP treatment (Figure 3A). CCCP-treated VPS35^{D620N} cells showed less colocalization between PINK1 and TOM20 compared to WT cells, and a dose-dependent effect of CCCP was observed (10 μM CCCP: WT median 0.12 vs. clone 1 median 0.04 and clone 2 0.05; 20 μM CCCP: WT median 0.52 vs. clone 1 median 0.36 and clone 2 median 0.35) (Figure 3B). Together, these data suggest that CCCP-induced PINK1 accumulation is hampered, leading to impaired Parkin recruitment onto mitochondria in VPS35^{D620N} cells.

CCCP-induced mitophagy is impaired in VPS35^{D620N} cells

To prove that the hampered PINK1 and Parkin recruitment onto mitochondria upon CCCP treatment does lead to compromised PINK1/Parkin-mediated mitophagy in VPS35^{D620N} cells, we used previously published dual color fluorescence-quenching EGFP-mCherry mitophagy reporter[39], which we stably expressed in WT and VPS35^{D620N} cells. Under normal conditions, mitochondria emit both a red and green fluorescence signal, which results in a yellow color (Figure 4A). Mitochondria damaged by CCCP treatment are transported to lysosomes for degradation, and the EGFP fluorescent signal is quenched within this acidic organelle, leaving mainly a red fluorescent signal (Figure 4A, B). At steady state, both WT and VPS35^{D620N} cells primarily showed a yellow reticulated mitochondrial network, with only a few red-only puncta, probably reflecting mitochondria within lysosomes, i.e. mitolysosomes, and there was no significant difference between the cell lines (Figure 4A, B). In contrast, while WT cells showed a substantial increase in mitochondria with a red-only signal, indicative of an activation of mitophagy[39], VPS35^{D620N} cells did not display a shift from yellow to red-only mitochondria after 24 hours of 10 µM CCCP treatment (Figures 4A, B). Interestingly, a punctate rearrangement of the mitochondrial network was observed in VPS35^{D620N} cells after CCCP treatment, in which the mitochondrial clumps seemed larger compared to WT cells (Figure 4A, bottom right panel compared to bottom left panel). This suggests that VPS35^{D620N} cells do react to CCCP but experience impairment in PINK1/Parkin-mediated mitophagy.

To confirm this finding, we investigated mitophagy using a different approach by transiently transfecting WT and VPS35^{D620N} cells with EGFP-LC3, a protein marker for autophagosomes[46]. Mitophagy was induced by 10 µM CCCP treatment for 6 hours, and we subsequently used IF to examine the colocalization between LC3 puncta, which represent autophagosomes, and TOM20 (Figure 4C, arrowheads). CCCP treatment in WT cells led to approximately twice the amount of LC3- and TOM20-positive mitophagosomes compared to VPS35^{D620N} cells (Figure 4D). Moreover, multiple VPS35^{D620N} cells did not form TOM20-positive autophagosomes, a phenomenon rarely seen in WT cells (Figure 4D). Altogether, these results confirm that CCCP-induced mitophagy is impaired in VPS35^{D620N} cells.

VPS35^{D620N} cells accumulate PINK1 in response to mitochondrial depolarization via antimycin A and oligomycin

Next, we questioned if PINK1/Parkin-mediated mitophagy in VPS35^{D620N} cells would be impaired by treatment with two agents that, like CCCP, also lead to substantial mitochondrial depolarization: subcomplex III inhibitor antimycin A and F_1F_0 ATPase inhibitor oligomycin[47]. Antimycin A causes a collapse of the proton gradient across the inner mitochondrial membrane by blocking the mitochondrial electron transport chain, whereas oligomycin inhibits the flow of protons through F_1F_0 ATPase inhibition, leading to a complete $\Delta\psi_m$ collapse. As shown using immunoblotting, antimycin A (1 µM, 24 hours) alone was not sufficient to stabilize PINK1 levels in WT cells, while treatment with oligomycin (1 µM, 24 hours) did (Figure 5A). As seen with CCCP, the oligomycin-treated VPS35^{D620N} cells showed less accumulation of PINK1 and higher levels of Parkin compared to WT (Figure 5A). Notably, co-incubation

with AO caused high PINK1 accumulation and loss of Parkin in both WT and VPS35^{D620N} cells, and in a similar manner. To corroborate this finding, mitochondrial PINK1 accumulation was determined using IF after 24 hours of 1 μM AO treatment (Figure 5B). In agreement with our immunoblotting data, PINK1 colocalized with TOM20 in almost all WT and VPS35^{D620N} cells, and no differences in the level of colocalization were observed between the different cell lines (Figure 5C). Finally, we monitored AO-induced mitophagy using the dual color mitophagy reporter stably expressed in WT and VPS35^{D620N} cells and observed no differences (Figure 5D). Together, these findings show that PINK1/Parkin recruitment and mitophagy can occur in VPS35^{D620N} cells in response to specific kinds of mitochondrial damage. However, the type and/or severity of insult to the mitochondrial membrane potential determines whether or not PINK1/Parkin-mediated mitophagy is initiated in VPS35^{D620N} cells.

Altered mitochondrial membrane potential and response to CCCP treatment in VPS35^{D620N} cells

To investigate whether AO treatment caused a different type of mitochondrial damage than CCCP treatment, we examined the rearrangement of the mitochondrial network upon exposure to these treatments. To do so, we analyzed the TOM20 distribution using IF to study the morphological characteristics of mitochondria including the number, aspect ratio and length of mitochondria in AO- and CCCP-treated cells (Figure 6A–C). Both treatments caused mitochondrial fragmentation, as evidenced by a substantial increase in mitochondrial particles (Figure 6A) and decreases in aspect ratio (Figure 6B) and mitochondrial length (Figure 6C). However, AO treatment led to more fragmentation than CCCP treatment, as the number of mitochondrial particles was significantly higher (Figure 6A). Additionally, and in line with our previous results, no differences were observed between WT and VPS35^{D620N} cells upon AO treatment. Interestingly, upon CCCP-treatment, the mitochondrial particles appeared less rounded and longer, as reflected by the increase in aspect ratio and length, respectively, in VPS35^{D620N} cells compared to WT cells (Figure 6A-C). These data suggest that mitochondria respond differently to AO and CCCP treatment and that AO causes more severe mitochondrial damage/fragmentation than CCCP. Additionally, the mitochondria in VPS35^{D620N} cells are affected by the treatments, i.e. they display mitochondrial fragmentation, albeit to a lesser extent than in WT cells.

To further explore why VPS35^{D620N} cells are affected by CCCP-induced damage but do not activate PINK1/Parkin mitophagy, we investigated the $\Delta\psi_m$ collapse upon CCCP treatment. The $\Delta\psi_m$ collapse triggers mitochondrial fragmentation, PINK1 accumulation on mitochondria and induction mitophagy[21,29]. $\Delta\psi_m$ was measured with the cell-permeant fluorescent dye TMRM in WT and VPS35^{D620N} cells over time upon treatment with 10 μM CCCP. Although CCCP treatment rapidly decreased $\Delta\psi_m$ in both WT and VPS35^{D620N} cells after 1 minute, and $\Delta\psi_m$ gradually decreased further during the next 19 minutes (Figure 6D), the collapse in $\Delta\psi_m$ was significantly lower in VPS35^{D620N} cells compared to WT cells at all measured time points. Additionally, VPS35^{D620N} cells exhibited a lower $\Delta\psi_m$ at resting condition (±25% less) compared to WT cells (Figure 6E). These data reveal that the mitochondrial

membrane potential in the mitochondria of VPS35^{D620N} cells is already altered at steady state and point to an altered mitochondrial susceptibility to CCCP treatment.

VPS35^{D620N} cells exhibit increased mitochondrial fragmentation and damage at steady state

Given that our IF data on mitochondrial distribution showed results inconsistent with previous reports about cells (over)expressing VPS35^{D620N}[14,15], likely due to resolution limitations, we used TEM to study WT and VPS35^{D620N} cells at steady state and under CCCP-treated conditions (10 µM CCCP for 6 hours). Here we observed that VPS35^{D620N} cells already had smaller, fragmented mitochondria compared to WT cells at steady state (Figure 7A), something that we had not observed with IF, probably due to the different resolutions of these two experimental approaches. CCCP treatment led to mitochondrial fragmentation in WT cells that resembled the mitochondrial phenotype of VPS35^{D620N} cells at steady state (Figure 7A, B). Notably, no further mitochondrial fragmentation was detected in CCCP-treated VPS35^{D620N} cells compared to the mitochondrial fragmentation seen in VPS35^{D620N} cells at steady state (Figure 7B).

Furthermore, five morphologically distinct categories of mitochondria were observed in the various samples (Figure 7C): I) classical healthy mitochondria with well-defined cristae, II) swollen mitochondria with defined cristae and dark in content, III) mitochondria with unclear, partially visible cristae, IV) mitochondria with very dark content and no visible cristae, and V) aberrant mitochondria with remnants of cristae and light in content. We quantified the proportion of these categories in WT and VPS35^{D620N} cells at steady state and after CCCP treatment. At steady state, most mitochondria (~84%) in WT cells were category I, and the remainder were category II (~9%) and III (~5%). In contrast, in VPS35^{D620N} cells at steady state, a large fraction (~45%) of the mitochondria were in category II, and we observed significantly fewer healthy category I mitochondria compared to WT cells (Figure 7D). Upon CCCP treatment, we observed a shift from category I (~60%) to category II (~26%) mitochondria in WT cells, as well as an increase in category IV mitochondria (from ~1% to ~9%). This suggests that category II mitochondria are damaged. Intriguingly, CCCP treatment did not cause a compositional shift in the mitochondrial population of VPS35^{D620N} cells. These data show that VPS35^{D620N} cells at steady state already contain a population of damaged and fragmented mitochondria and, in agreement with our other results, confirm that this population of mitochondria does not respond further to CCCP treatment.

Discussion

In the present study, we show for the first time that the actions of VPS35 converge on the PINK1/Parkin pathway and that VPS35^{D620N} cells show deficits in CCCP-induced PINK1/Parkin-mediated mitophagy. Importantly, these data have been acquired using a model that closely mimics the situation in PD patients. Mitochondria of VPS35^{D620N} cells seem desensitized to a CCCP-induced $\Delta\psi_m$ collapse, as they appear already damaged/fragmented and have a reduced mitochondrial membrane potential at steady state. Consequently, mitochondria of CCCP-treated VPS35^{D620N} cells show almost no accumulation of PINK1 and Parkin, and therefore fail to initiate mitophagy. However, PINK1/Parkin-dependent mitophagy

in VPS35^{D620N} cells is still operational, as VPS35^{D620N} cells display PINK1/Parkin-mediated mitophagy upon strong mitochondrial depolarization events induced by AO treatment. We suggest that the mitochondria of VPS35^{D620N} already exhibit a specific type of damage at steady state. This renders them insensitive to CCCP and likely also to other stressors that may initiate PINK1/Parkin-mediated mitophagy in humans. We speculate that individuals carrying the p.D620N variant in VPS35 may tend to accumulate damaged mitochondria because of this impairment, and, over time, this could cause neurodegeneration.

The observed failure of VPS35^{D620N} cells to maintain $\Delta\psi_m$ under steady state is likely linked to the presence of damaged mitochondria and will have deleterious effects on cell viability and functions, as $\Delta\psi_m$ provides the driving force for ATP synthesis[48]. Maintenance of $\Delta\psi_m$ is important for the inward transport of cations such as Ca^{2+}[49] and necessary for the import of numerous mitochondrial proteins[50,51]. Mitochondrial quality control mechanisms that maintain $\Delta\psi_m$, such as mitochondrial fragmentation[52] or the removal of depolarized mitochondria through mitophagy[29,53], are thus essential and are likely affected in VPS35^{D620N} cells, which leads to the observed accumulation of damaged and fragmented mitochondria under steady state conditions. Importantly, while this manuscript was in preparation, another study was published showing that p.D620N-mutant VPS35 patient-derived dopaminergic neurons also exhibit mitochondrial impairments, including a reduction in $\Delta\psi_m$ under steady state, and present defects in CCCP-induced mitophagy, thereby confirming our results[54]. Moreover, depletion of VPS35 in neuroblastoma cells also causes reduced basal $\Delta\psi_m$ and an increase in mitochondrial fission at steady state[15]. Notably, similar defects in maintenance of $\Delta\psi_m$ and mitochondrial dynamics have been observed in other models for PD, including those for PINK1 and Parkin[55,56].

Our data also suggest that VPS35^{D620N} cells are less able to respond to a collapse in $\Delta\psi_m$, as indicated by the reduced PINK1/Parkin-mediated mitophagy upon $\Delta\psi_m$ loss due to CCCP treatment. The fact that AO treatment was able to induce PINK1/Parkin-mediated mitophagy in VPS35^{D620N} cells while CCCP could not can be explained by the difference in how the compounds affect mitochondrial depolarization. CCCP dissipates $\Delta\psi_m$ by removing the proton gradient over the mitochondrial membrane by increasing the permeability of protons across the inner mitochondrial membrane. As such, the duration and the amount of CCCP dictates the extent of $\Delta\psi_m$ loss, and consequently the amount of PINK1 stabilization and accumulation. Antimycin A and oligomycin both block the function of the mitochondrial electron transport chain, which actively maintains the $\Delta\psi_m$, causing a loss of $\Delta\psi_m$. Oligomycin also blocks the reverse ATP synthase activity of the F_1F_0 ATPase, which is normally utilized to counteract loss of $\Delta\psi_m$ by actively pumping protons into the intermembrane space, thereby causing a further decrease in $\Delta\psi_m$[57,58]. Importantly, differences in the level of mitochondrial depolarization between CCCP and AO have been reported before[59]. Thus, it is likely that in VPS35^{D602N} cells, which already have a lower $\Delta\psi_m$ at steady state conditions, the $\Delta\psi_m$ collapses induced by CCCP are too small to provoke additional mitochondrial fragmentation and thereby induce PINK1/Parkin-mediated mitophagy.

So why is PINK1/Parkin-mediated mitophagy impaired in VPS35^{D620N} cells upon CCCP treatment? We hypothesize that, since VPS35^{D620N} cells already display loss of $\Delta\psi_m$ at steady state, PINK1/Parkin-mediated mitophagy may not be activated upon mild stress in order to prevent continuous turnover of mildly damaged mitochondria, i.e. these cells exhibit desensitization to prevent depletion of the mitochondrial pool. Although we did not elucidate how VPS35 modifies PINK1/Parkin-mediated mitophagy, our data advocates that this impairment is associated with the already damaged/fragmented mitochondria with lower $\Delta\psi_m$ in VPS35^{D620N} cells at steady state.

Furthermore, as our study focused only on PINK1/Parkin-mediated mitophagy, we cannot rule out that other forms of mitophagy are affected in VPS35^{D620N} cells. Of note, multiple studies have shown that mitophagy can be induced with CCCP via other ubiquitin E3 ligases, independent of Parkin[60,61]. Moreover, receptor-mediated mitophagy can occur without ubiquitin E3 ligases through direct interactions of autophagic receptors present on the OMM with LC3, thereby circumventing the PINK1/Parkin pathway[62,63]. Future studies are necessary to investigate whether these alternative routes of mitophagy induction are also affected in VPS35^{D620N} cells.

The established role of VPS35 and retromer in mitochondrial physiology is to retrieve mitochondrial proteins via MDVs[13], and it has been shown that the D620N variant in *VPS35* affects the sorting of MUL1 and DLP1[14,16]. With the expanding research on the proteome of MDVs[64], it is likely that retromer is involved in trafficking of additional mitochondrial proteins. To what extent this is regulated by retromer and, importantly, which cargoes are being transported is unclear. However, the sorting of other mitochondrial proteins is probably affected and could cause the mitochondrial impairments, e.g. damage/fragmentation, in VPS35^{D620N} cells. For example, the loss of $\Delta\psi_m$ in VPS35^{D620N} cells may be caused by changes in regulatory proteins involved in maintaining $\Delta\psi_m$, such as the mitochondrial permeability transition pore complex or components of the oxidative phosphorylation machinery[64,65]. In addition, a recent study showed that VPS35 interacts with Parkin, suggesting that members of the PINK1/Parkin-pathway are directly affected by VPS35-mediated MDV trafficking[66]. Although a role for VPS35 in MDV transport has been established[13,14], the field of MDV-mediated transport is still emerging and many questions remain regarding their role in mitochondrial quality control and regulation of different cargoes[67].

Conclusion

Our data show that the D620N variant in *VPS35* leads to mitochondrial defects that affect PINK1/Parkin-mediated mitophagy. This finding supports the notion that multiple familial PD genes converge in similar pathways and further extends our knowledge about the general disease mechanisms of PD.

Abbreviations

AO: Antimycin A and Oligomycin

CCCP: carbonyl cyanide m-chlorophenyl hydrazone

IF: Immunofluorescence

PD: Parkinson's disease

TEM: Transmission electron microscopy

TMRM: tetramethyl-rhodamine, methyl ester

$\Delta\psi_m$: Mitochondrial membrane potential

WT: Wild type

Declarations

Ethics approval and consent to participate

Not applicable.

Consent for publication

Not applicable

Availability of data and materials

The raw data and fluorescence images are available from the corresponding authors upon reasonable request.

Competing interests

The authors declare no competing interests.

Funding

D.S.V. is supported by a Rosalind Franklin Fellowship from the University of

Groningen (UG). K.Y.M. is supported by the Jan Kornelis de Cock-Stichting and the U4 PhD program of the Behavioral and Cognitive Neuroscience graduate school of the UG. M.M. is supported by an ALW Open Programme (ALWOP.355). F.R. is supported by ZonMW TOP (91217002), ALW Open Programme (ALWOP.310), Open Competition ENW-KLEIN (OCENW.KLEIN.118), Marie Skłodowska-Curie Cofund (713660) and Marie Skłodowska Curie ETN (765912) grants. Part of this work was performed at the University Medical Centre Groningen Microscopy and Imaging Centre, which is sponsored by the Netherlands Organization for Scientific Research (NWO grants 40-00506-98-9021 and 175-010-2009-

023). None of the funding bodies were involved in the collection, analysis and interpretation of data, nor in the writing of the manuscript.

Authors' Contributions

K.Y.M. conceived and designed the project, created the cell lines, performed all *in vitro*

experiments and fluorescence microscopy, analyzed the data and wrote the manuscript. M.R.F. participated in creating the cell lines and performed cloning of the mitophagy reporter vector. M.M. performed transmission electron microscopy and analyzed these data. F.R. participated in the interpretation of results and helped in revising the manuscript. D.S.V. designed and supervised the project, participated in the interpretation of results and wrote and revised the manuscript. All authors read and approved the final manuscript.

Acknowledgements

We would like to thank Kate McIntyre for editing this manuscript.

References

1. Tysnes O-B, Storstein A. Epidemiology of Parkinson's disease. *J Neural Transm*. 2017;124(8):901-905. doi:10.1007/s00702-017-1686-y
2. Valente EM, Abou-Sleiman PM, Caputo V, et al. Hereditary early-onset Parkinson's disease caused by mutations in PINK1. *Science (80-)*. 2004;304(5674):1158-1160. doi:10.1126/science.1096284
3. Kitada T, Asakawa S, Hattori N, et al. Mutations in the parkin gene cause autosomal recessive juvenile parkinsonism. *Nature*. 1998;392(6676):605-608. doi:10.1038/33416
4. Vilariño-Güell C, Wider C, Ross OA, et al. VPS35 mutations in parkinson disease. *Am J Hum Genet*. 2011;89(1):162-167. doi:10.1016/j.ajhg.2011.06.001
5. Zimprich A, Benet-Pages A, Struhal W, et al. A Mutation in VPS35, Encoding a Subunit of the Retromer Complex, Causes Late-Onset Parkinson Disease. *Am J Hum Genet*. 2011;89(1):168-175. doi:10.1016/j.ajhg.2011.06.008
6. Williams ET, Chen X, Moore DJ. VPS35, the retromer complex and Parkinson's disease. *J Parkinsons Dis*. 2017;7(2):219-233. doi:10.3233/JPD-161020
7. Hierro A, Rojas AL, Rojas R, et al. Functional architecture of the retromer cargo-recognition complex. *Nature*. 2007;449(7165):1063-1067. doi:10.1038/nature06216
8. Burd C, Cullen PJ. Retromer: A master conductor of endosome sorting. *Cold Spring Harb Perspect Biol*. 2014;6(2). doi:10.1101/cshperspect.a016774
9. Zavodszky E, Seaman MN, Rubinsztein DC. VPS35 Parkinson mutation impairs autophagy via WASH. *Cell Cycle*. 2014;13(14):2155-2156. doi:10.4161/cc.29734

10. McGough IJ, Steinberg F, Jia D, et al. Retromer binding to FAM21 and the WASH complex is perturbed by the Parkinson disease-linked VPS35(D620N) mutation. *Curr Biol*. 2014;24(14):1670-1676. doi:10.1016/j.cub.2014.06.024
11. Munsie LN, Milnerwood AJ, Seibler P, et al. Retromer-dependent neurotransmitter receptor trafficking to synapses is altered by the Parkinson's disease VPS35 mutation p.D620N. *Hum Mol Genet*. 2015;24(6):1691-1703. doi:10.1093/hmg/ddu582
12. Follett J, Norwood SJ, Hamilton NA, et al. The Vps35 D620N Mutation Linked to Parkinson's Disease Disrupts the Cargo Sorting Function of Retromer. *Traffic*. 2014;15(2):230-244. doi:10.1111/tra.12136
13. Braschi E, Goyon V, Zunino R, Mohanty A, Xu L, McBride HM. Vps35 Mediates Vesicle Transport between the Mitochondria and Peroxisomes. *Curr Biol*. 2010;20(14):1310-1315. doi:10.1016/J.CUB.2010.05.066
14. Wang W, Wang X, Fujioka H, et al. Parkinson's disease-associated mutant VPS35 causes mitochondrial dysfunction by recycling DLP1 complexes. *Nat Med*. 2016;22(1):54-63. doi:10.1038/nm.3983
15. Tang F-L, Liu W, Hu J-X, et al. VPS35 Deficiency or Mutation Causes Dopaminergic Neuronal Loss by Impairing Mitochondrial Fusion and Function. *Cell Rep*. 2015;12(10):1631-1643. doi:10.1016/J.CELREP.2015.08.001
16. Wang W, Ma X, Zhou L, Liu J, Zhu X. A conserved retromer sorting motif is essential for mitochondrial DLP1 recycling by VPS35 in Parkinson's disease model. *Hum Mol Genet*. 2016;26(4):ddw430. doi:10.1093/hmg/ddw430
17. Bose A, Beal MF. Mitochondrial dysfunction in Parkinson's disease. *J Neurochem*. 2016;139(S1):216-231. doi:10.1111/jnc.13731
18. Abou-Sleiman PM, Muqit MMK, Wood NW. Expanding insights of mitochondrial dysfunction in Parkinson's disease. *Nat Rev Neurosci*. 2006;7(3):207-219. doi:10.1038/nrn1868
19. Ryan BJ, Hoek S, Fon EA, Wade-Martins R. Mitochondrial dysfunction and mitophagy in Parkinson's: from familial to sporadic disease. *Trends Biochem Sci*. 2015;40(4):200-210. doi:10.1016/J.TIBS.2015.02.003
20. Matsuda N, Sato S, Shiba K, et al. PINK1 stabilized by mitochondrial depolarization recruits Parkin to damaged mitochondria and activates latent Parkin for mitophagy. *J Cell Biol*. 2010;189(2):211-221. doi:10.1083/jcb.200910140
21. Narendra DP, Jin SM, Tanaka A, et al. PINK1 is selectively stabilized on impaired mitochondria to activate Parkin. *PLoS Biol*. 2010;8(1). doi:10.1371/journal.pbio.1000298
22. Geisler S, Holmström KM, Treis A, et al. The PINK1/Parkin-mediated mitophagy is compromised by PD-associated mutations. *Autophagy*. 2010;6(7):871-878. doi:10.4161/auto.6.7.13286
23. Greene AW, Grenier K, Aguileta MA, et al. Mitochondrial processing peptidase regulates PINK1 processing, import and Parkin recruitment. *EMBO Rep*. 2012;13(4):378-385. doi:10.1038/embor.2012.14

24. Narendra D, Tanaka A, Suen DF, Youle RJ. Parkin is recruited selectively to impaired mitochondria and promotes their autophagy. *J Cell Biol*. 2008;183(5):795-803. doi:10.1083/jcb.200809125
25. Kim Y, Park J, Kim S, et al. PINK1 controls mitochondrial localization of Parkin through direct phosphorylation. *Biochem Biophys Res Commun*. 2008;377(3):975-980. doi:10.1016/j.bbrc.2008.10.104
26. Lazarou M, Sliter DA, Kane LA, et al. The ubiquitin kinase PINK1 recruits autophagy receptors to induce mitophagy. *Nature*. 2015;524(7565):309-314. doi:10.1038/nature14893
27. Scarffe LA, Stevens DA, Dawson VL, Dawson TM. Parkin and PINK1: Much more than mitophagy. *Trends Neurosci*. 2014;37(6):315-324. doi:10.1016/j.tins.2014.03.004
28. Geisler S, Holmström KM, Skujat D, et al. PINK1/Parkin-mediated mitophagy is dependent on VDAC1 and p62/SQSTM1. *Nat Cell Biol*. 2010;12(2):119-131. doi:10.1038/ncb2012
29. Youle RJ, Narendra DP. Mechanisms of mitophagy. *Nat Rev Mol Cell Biol*. 2011;12(1):9-14. doi:10.1038/nrm3028
30. Palikaras K, Lionaki E, Tavernarakis N. Mechanisms of mitophagy in cellular homeostasis, physiology and pathology. *Nat Cell Biol*. 2018;20(9). doi:10.1038/s41556-018-0176-2
31. McWilliams TG, Prescott AR, Allen GFG, et al. Mito-QC illuminates mitophagy and mitochondrial architecture in vivo. *J Cell Biol*. 2016;214(3):333-345. doi:10.1083/jcb.201603039
32. McWilliams TG, Prescott AR, Montava-Garriga L, et al. Basal Mitophagy Occurs Independently of PINK1 in Mouse Tissues of High Metabolic Demand. *Cell Metab*. 2018;27(2):439-449.e5. doi:10.1016/j.cmet.2017.12.008
33. Lee JJ, Sanchez-Martinez A, Zarate AM, et al. Basal mitophagy is widespread in Drosophila but minimally affected by loss of Pink1 or parkin. *J Cell Biol*. 2018;217(5):1613-1622. doi:10.1083/jcb.201801044
34. Pickrell AM, Huang CH, Kennedy SR, et al. Endogenous Parkin Preserves Dopaminergic Substantia Nigral Neurons following Mitochondrial DNA Mutagenic Stress. *Neuron*. 2015;87(2):371-381. doi:10.1016/j.neuron.2015.06.034
35. Guzman JN, Sanchez-Padilla J, Wokosin D, et al. Oxidant stress evoked by pacemaking in dopaminergic neurons is attenuated by DJ-1. *Nature*. 2010;468(7324). doi:10.1038/nature09536
36. Trempe JF, Sauvé V, Grenier K, et al. Structure of parkin reveals mechanisms for ubiquitin ligase activation. *Science (80-)*. 2013;340(6139):1451-1455. doi:10.1126/science.1237908
37. In HL, Cao L, Mostoslavsky R, et al. A role for the NAD-dependent deacetylase Sirt1 in the regulation of autophagy. *Proc Natl Acad Sci U S A*. 2008;105(9):3374-3379. doi:10.1073/pnas.0712145105
38. Ran FA, Hsu PD, Wright J, Agarwala V, Scott DA, Zhang F. Genome engineering using the CRISPR-Cas9 system. *Nat Protoc*. 2013;8(11):2281-2308. doi:10.1038/nprot.2013.143
39. Rojansky R, Cha MY, Chan DC. Elimination of paternal mitochondria in mouse embryos occurs through autophagic degradation dependent on PARKIN and MUL1. *Elife*. 2016;5(NOVEMBER2016). doi:10.7554/eLife.17896

40. Almeida A, Medina JM. A rapid method for the isolation of metabolically active mitochondria from rat neurons and astrocytes in primary culture. *Brain Res Protoc*. 1998;2(3):209-214. doi:10.1016/S1385-299X(97)00044-5
41. Costes S V., Daelemans D, Cho EH, Dobbin Z, Pavlakis G, Lockett S. Automatic and quantitative measurement of protein-protein colocalization in live cells. *Biophys J*. 2004;86(6):3993-4003. doi:10.1529/biophysj.103.038422
42. Cribbs JT, Strack S. Reversible phosphorylation of Drp1 by cyclic AMP-dependent protein kinase and calcineurin regulates mitochondrial fission and cell death. *EMBO Rep*. 2007;8(10):939-944. doi:10.1038/sj.embor.7401062
43. Verheije MH, Raaben M, Mari M, et al. Mouse Hepatitis Coronavirus RNA Replication Depends on GBF1-Mediated ARF1 Activation. Baric RS, ed. *PLoS Pathog*. 2008;4(6):e1000088. doi:10.1371/journal.ppat.1000088
44. Xicoy H, Wieringa B, Martens GJM. The SH-SY5Y cell line in Parkinson's disease research: a systematic review. *Mol Neurodegener*. 2017;12(1):1-11. doi:10.1186/s13024-017-0149-0
45. Rakovic A, Shurkewitsch K, Seibler P, et al. Phosphatase and tensin homolog (PTEN)-induced Putative Kinase 1 (PINK1)-dependent ubiquitination of endogenous parkin attenuates mitophagy: Study in human primary fibroblasts and induced pluripotent stem cell-derived neurons. *J Biol Chem*. 2013;288(4):2223-2237. doi:10.1074/jbc.M112.391680
46. Klionsky DJ, Abdelmohsen K, Abe A, et al. Guidelines for the use and interpretation of assays for monitoring autophagy (3rd edition).[Erratum appears in Autophagy. 2016;12(2):443 Note: Selliez, Iban [corrected to Seiliez, Iban]; PMID: 26902590]. 2016. http://ovidsp.ovid.com/ovidweb.cgi?T=JS&CSC=Y&NEWS=N&PAGE=fulltext&D=medc&AN=26799652. Accessed September 9, 2019.
47. Vives-Bauza C, Zhou C, Huang Y, et al. PINK1-dependent recruitment of Parkin to mitochondria in mitophagy. *Proc Natl Acad Sci U S A*. 2010;107(1):378-383. doi:10.1073/pnas.0911187107
48. Klingenberg M, Rottenberg H. Relation between the Gradient of the ATP/ADP Ratio and the Membrane Potential across the Mitochondrial Membrane. *Eur J Biochem*. 1977;73(1):125-130. doi:10.1111/j.1432-1033.1977.tb11298.x
49. Gunter TE, Pfeiffer DR. Mechanisms by which mitochondria transport calcium. *Am J Physiol - Cell Physiol*. 1990;258(5 27-5). doi:10.1152/ajpcell.1990.258.5.c755
50. Shariff K, Ghosal S, Matouschek A. The force exerted by the membrane potential during protein import into the mitochondrial matrix. *Biophys J*. 2004;86(6):3647-3652. doi:10.1529/biophysj.104.040865
51. Krayl M, Lim JH, Martin F, Guiard B, Voos W. A Cooperative Action of the ATP-Dependent Import Motor Complex and the Inner Membrane Potential Drives Mitochondrial Preprotein Import. *Mol Cell Biol*. 2007;27(2):411-425. doi:10.1128/mcb.01391-06
52. Ishihara N, Jofuku A, Eura Y, Mihara K. Regulation of mitochondrial morphology by membrane potential, and DRP1-dependent division and FZO1-dependent fusion reaction in mammalian cells. *Biochem Biophys Res Commun*. 2003;301(4):891-898. doi:10.1016/S0006-291X(03)00050-0

53. Pickles S, Vigié P, Youle RJ. Mitophagy and Quality Control Mechanisms in Mitochondrial Maintenance. *Curr Biol*. 2018;28(4):R170-R185. doi:10.1016/j.cub.2018.01.004
54. Hanss Z, Larsen SB, Antony P, et al. Mitochondrial and Clearance Impairment in p. D620N VPS35 Patient-Derived Neurons. *Mov Disord*. November 2020:mds.28365. doi:10.1002/mds.28365
55. Wang HL, Chou AH, Wu AS, et al. PARK6 PINK1 mutants are defective in maintaining mitochondrial membrane potential and inhibiting ROS formation of substantia nigra dopaminergic neurons. *Biochim Biophys Acta - Mol Basis Dis*. 2011;1812(6):674-684. doi:10.1016/j.bbadis.2011.03.007
56. Yu W, Sun Y, Guo S, Lu B. The PINK1/Parkin pathway regulates mitochondrial dynamics and function in mammalian hippocampal and dopaminergic neurons. *Hum Mol Genet*. 2011;20(16):3227-3240. doi:10.1093/hmg/ddr235
57. Lefebvre V, Du Q, Baird S, et al. Genome-wide RNAi screen identifies ATPase inhibitory factor 1 (ATPIF1) as essential for PARK2 recruitment and mitophagy) Genome-wide RNAi screen identifies ATPase inhibitory factor 1 (ATPIF1) as essential for PARK2 recruitment and mitophagy View supplementary material. *Autophagy*. 2013;9(11):1770-1779. doi:10.4161/auto.25413
58. Bornhö C, Vogel F, Neupert W, Reichert AS. Mitochondrial Membrane Potential Is Dependent on the Oligomeric State of F 1 F 0-ATP Synthase Supracomplexes * □ S. 2006. doi:10.1074/jbc.M512334200
59. Soutar MPM, Kempthorne L, Annuario E, et al. FBS/BSA media concentration determines CCCP's ability to depolarize mitochondria and activate PINK1-PRKN mitophagy. *Autophagy*. 2019;15(11):2002-2011. doi:10.1080/15548627.2019.1603549
60. Orvedahl A, Sumpter R, Xiao G, et al. Image-based genome-wide siRNA screen identifies selective autophagy factors. *Nature*. 2011;480(7375). doi:10.1038/nature10546
61. Fu M, St-Pierre P, Shankar J, Wang PTC, Joshi B, Nabi IR. Regulation of mitophagy by the Gp78 E3 ubiquitin ligase. *Mol Biol Cell*. 2013;24(8):1153-1162. doi:10.1091/mbc.E12-08-0607
62. Liu L, Feng D, Chen G, et al. Mitochondrial outer-membrane protein FUNDC1 mediates hypoxia-induced mitophagy in mammalian cells. *Nat Cell Biol*. 2012;14(2). doi:10.1038/ncb2422
63. Liu L, Sakakibara K, Chen Q, Okamoto K. Receptor-mediated mitophagy in yeast and mammalian systems. *Cell Res*. 2014;24(7). doi:10.1038/cr.2014.75
64. Roberts RF, Bayne AN, Goiran T, et al. Proteomic profiling of mitochondrial-derived vesicles in brain reveals enrichment of respiratory complex sub-assemblies and small TIM chaperones. doi:10.1101/2020.07.06.189993
65. Zorova LD, Popkov VA, Plotnikov EY, et al. Mitochondrial membrane potential. *Anal Biochem*. 2018;552:50-59. doi:10.1016/j.ab.2017.07.009
66. Williams ET, Glauser L, Tsika E, Jiang H, Islam S, Moore DJ. Parkin mediates the ubiquitination of VPS35 and modulates retromer-dependent endosomal sorting. *Hum Mol Genet*. 2018;27(18):3189-3205. doi:10.1093/hmg/ddy224
67. McLelland GL, Fon EA. Principles of mitochondrial vesicle transport. *Curr Opin Physiol*. 2018;3:25-33. doi:10.1016/j.cophys.2018.02.005

Figures

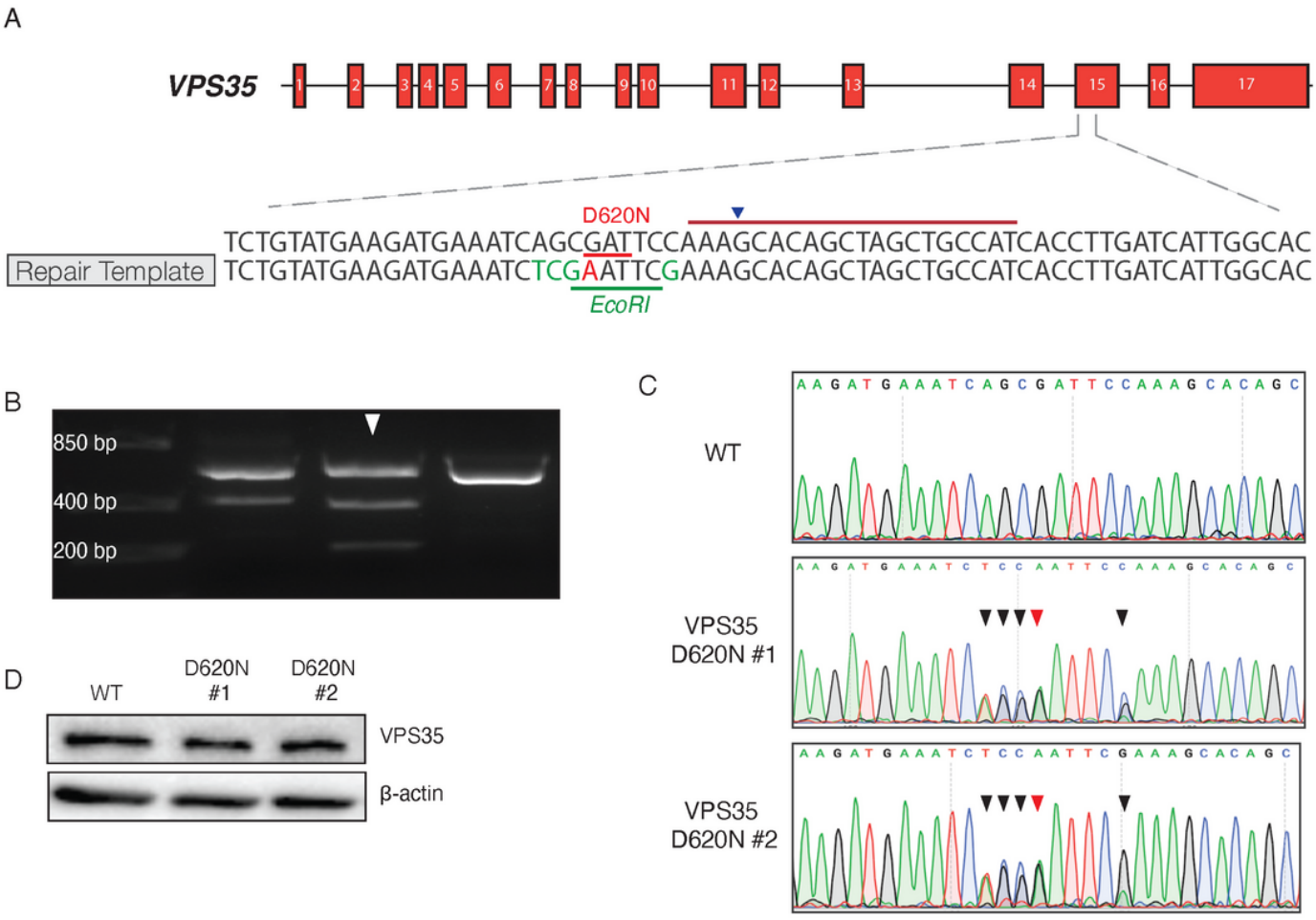

Figure 1

Generation of heterozygous VPS35D620N SH-SY5Y cells. A) Schematic representation of cloning strategy for the generation of the nucleotide exchange in the VPS35 locus that leads to the D620N mutation using CRISPR-Cas9 technology. Partial sequence of endogenous target on exon 15 is shown (upper sequence). 20-nt guide sequence is depicted by the burgundy line with the blue arrowhead pointing towards the predicted Cas9-cleavage site. GAT sequence that encodes the aspartic acid residue at position 620 is highlighted in red. Lower sequence shows the design of the repair template used to create the mutation. Patient substitution G>A is shown in red. Silent substitutions to create an EcoRI restriction site are shown in green. B) Representative agarose gel showing PCR products of the target VPS35 region obtained from different CRISPR-clones. PCR products were subjected to EcoRI digestion before loading on an agarose gel. Upper bands show noncleaved bands of the PCR amplicon. Arrowhead indicates an example of a successfully edited clone that was partially cleaved by EcoRI. C) Sanger chromatograms of the region surrounding the CRISPR-edit of WT (upper panel), VPS35 D620N clone 1 (middle panel) and VPS35 D620N clone 2 (lower panel). Red arrowhead indicates successful integration of the PD-

associated mutation G>A. Black arrowheads indicate silent substitutions to create the EcoRI restriction site. Note that double peaks are shown for the edited nucleotides as one allele remains unaltered. D) Representative immunoblots of protein extracts from WT and VPS35D620N (clone 1 and clone 2) cells. Blots were stained for VPS35 and β-actin (total protein loading control).

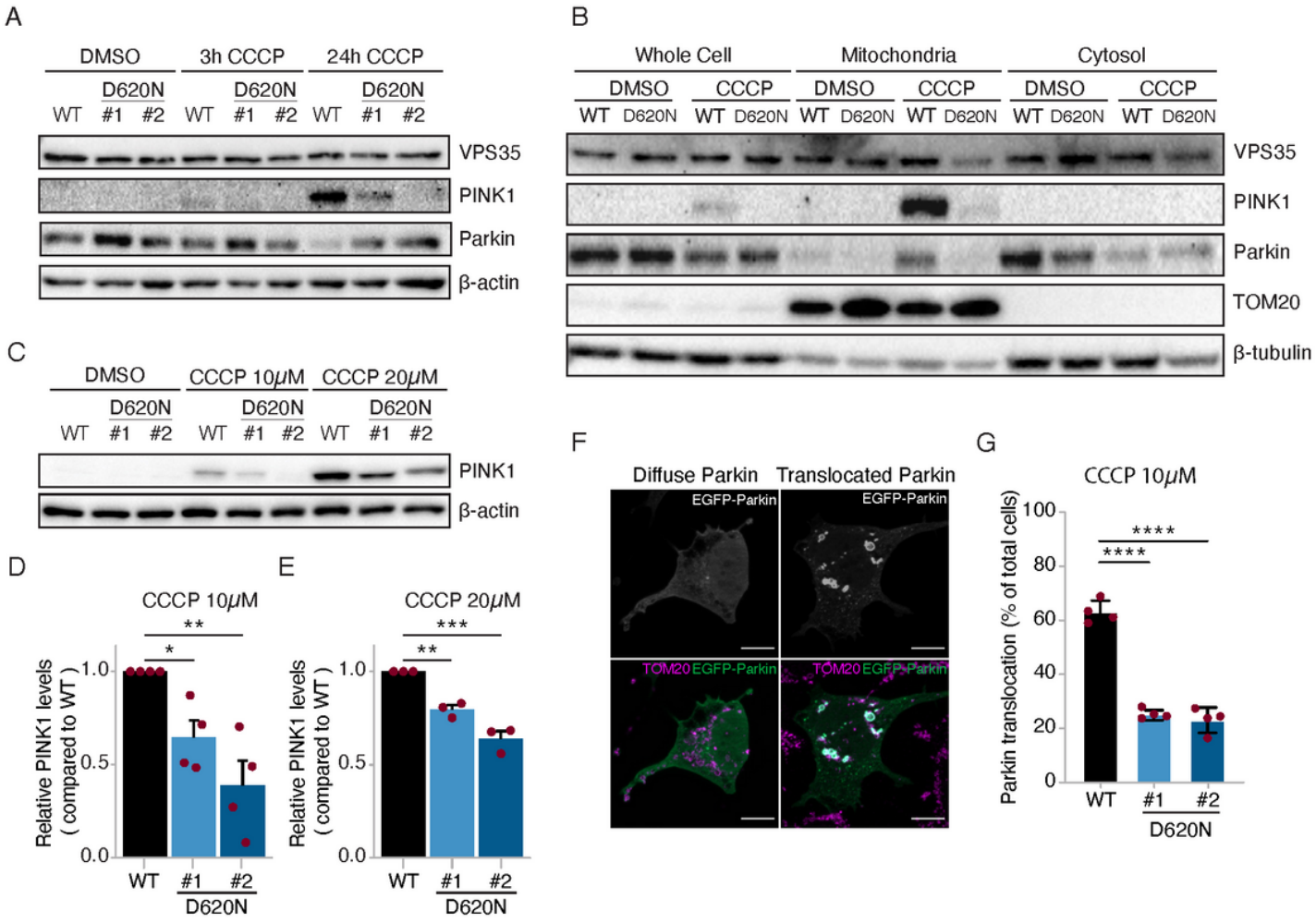

Figure 2

CCCP-induced PINK1/Parkin recruitment is impaired in VPS35D620N cells. A) Representative immunoblots of protein extracts from WT and VPS35 D620N (clone 1 and clone 2) SH-SY5Y cells treated with DMSO or 10 μM CCCP for 3 or 24 h. Blots were stained for VPS35, PINK1, Parkin and β-actin (total protein loading control) antibodies. B) Representative immunoblots of protein extracts derived from whole cell, crude mitochondrial fractions or cytosolic fraction from WT and VPS35D620N cells treated with either DMSO or 10 μM CCCP for 6 h. Blots were stained for VPS35, PINK1, Parkin, TOM20 (mitochondrial loading control) and β-actin (total protein loading control) antibodies. C) Representative immunoblots of protein extracts from WT and VPS35D620N (clone 1 and clone 2) cells treated with DMSO, 10 μM or 20 μM CCCP for 24 h. Blots were stained for PINK1 and β-actin (total protein loading control) antibodies. D-E) Quantification of PINK1 levels from immunoblot analysis in (C). Shown are relative PINK1 levels after 10 μM (D) or 20 μM CCCP (E) stimulation for 24 h compared to WT cells. Note

that PINK1 levels were not quantifiable when treated with DMSO and thus comparisons were made within each treatment condition. Each red dot depicts a separate experiment. Statistical analyses were performed by one-way ANOVA followed by a Tukey's post hoc test. F) Representative fluorescence images of cells transiently overexpressing EGFP-Parkin (upper panels: white, lower panels: green) also stained for the mitochondrial protein TOM20 (lower panels: magenta). Cells with a diffuse cytosolic distribution of EGFP-Parkin are depicted in the left panels and cells with EGFP-Parkin translocated onto mitochondria are shown in the right panels. Scale bar, 10 µm. G) Quantification of WT and VPS35D620N (clone 1 and clone 2) cells with EGFP-Parkin translocation to mitochondria, as shown in (F), after 10 µM CCCP stimulation for 24 h, represented as fraction (%) of all counted cells. Red dots represent the means of four different experiments in which at least 50 cells were counted. Data were analyzed using a beta regression. * $p < 0.05$, ** $p < 0.01$, *** $p < 0.005$, **** $p < 0.001$

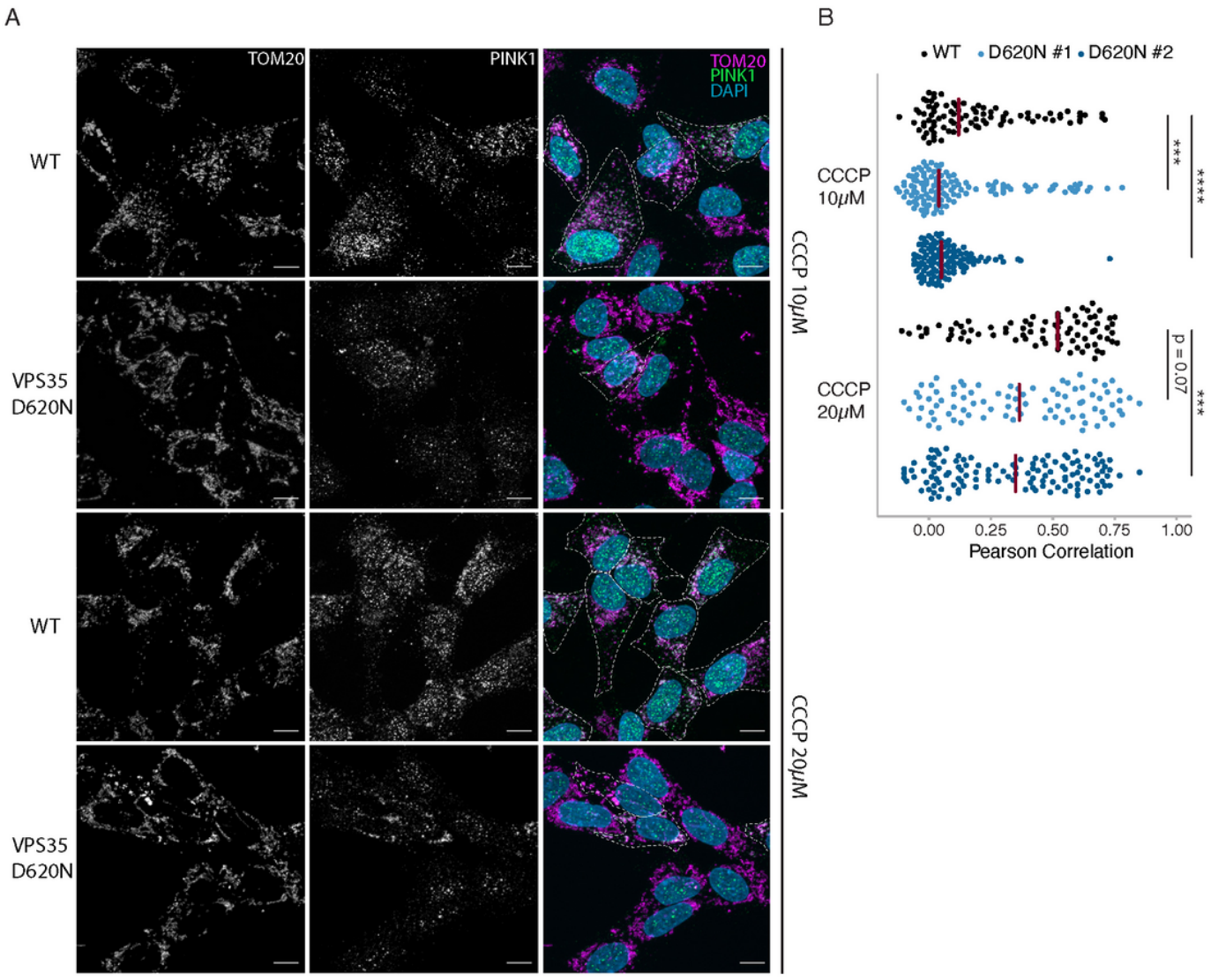

Figure 3

PINK1 does not localize to mitochondria upon CCCP treatment in VPS35D620N cells. A) Representative fluorescence images of WT or VPS35D620N cells treated with 10 µM or 20 µM CCCP for 24 h. Left panels show endogenous TOM20 staining. Middle panels show endogenous PINK1 staining. Right panels show the overlay image including DAPI staining for nuclei. Cells with co-localization (white) of TOM20 (magenta) and PINK1 (green) are outlined. Scale bar, 10 µm. B) Quantification of co-localization of endogenous TOM20 and PINK1 of WT and VPS35D620N (clone 1 and 2) cells treated with 10 µM or 20 µM CCCP for 24 h. Each dot represents the Pearson coefficient calculated for one cell. Red lines show the median Pearson coefficient per cell line. Statistical analyses were performed using the Kruskal-Wallis test followed by a pairwise Mann-Whitney U-test with Benjamini-Hochberg multiple testing correction. *** $p < 0.005$, **** $p < 0.001$

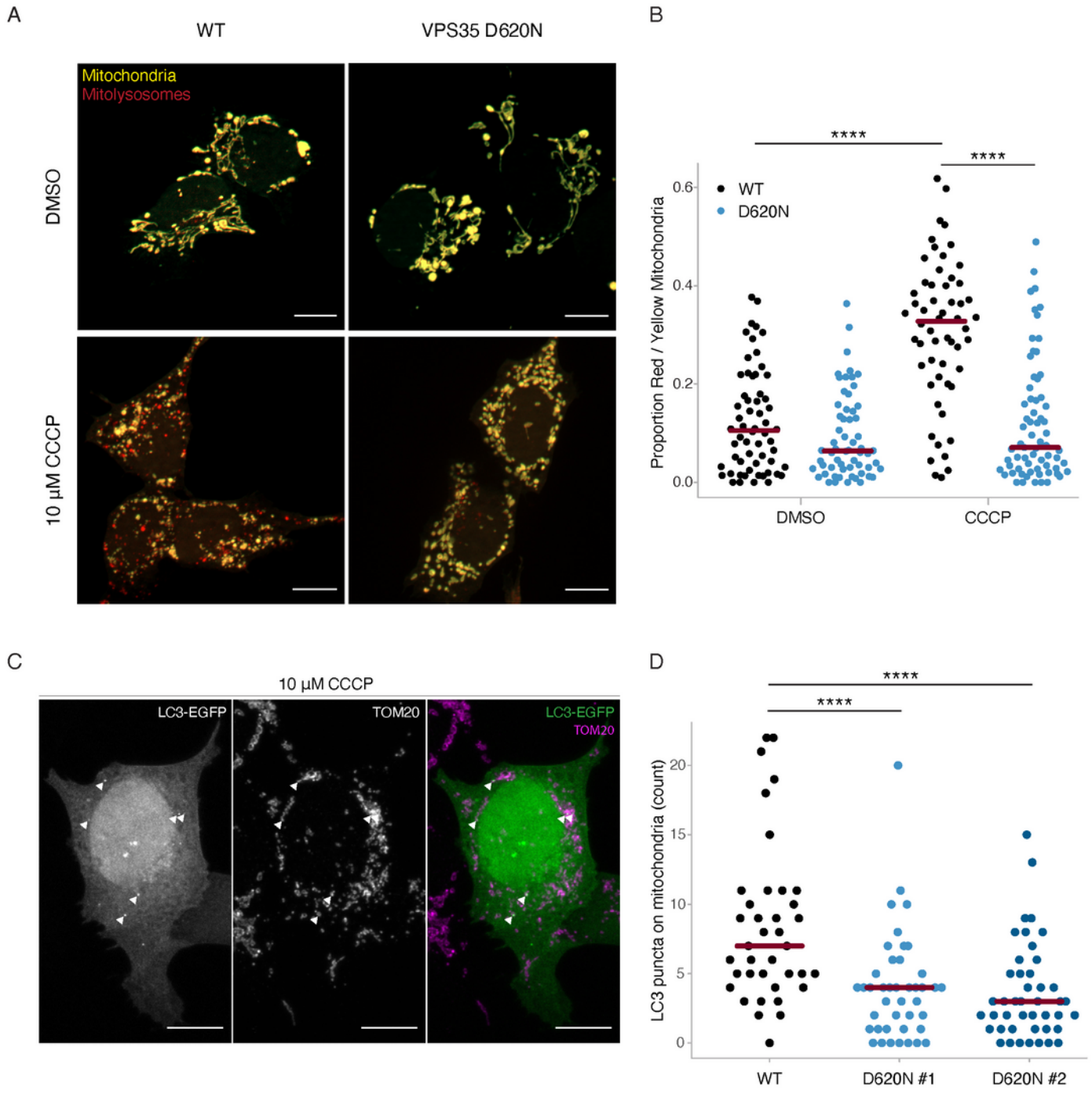

Figure 4

VPS35D620N cells display impaired mitophagy upon CCCP treatment. A) Representative fluorescence images of WT (left panels) or VPS35D620N (right panels) cells that stably express COX8-EGFP-mCherry treated with DMSO (upper panels) or 10 µM CCCP (lower panels) for 24 h. The signal from the yellow particles originate from EGFP and mCherry and highlights cytoplasmic mitochondria. The red particles show quenched EGFP signal and normal mCherry signal, reflecting mitochondria transported into an

acidic compartment (mitophagolysosome). Scale bar, 10 μm. B) Quantification of yellow and red particles in (A) in WT and VPS35 D620N cells treated with DMSO or 10 μM CCCP. Each dot represents the proportion of total yellow and red particles for one cell. Red lines show the median proportion per cell line per condition. Statistical analysis was performed using a beta regression. C) Representative confocal images of cells transiently overexpressing EGFP-LC3 (left panel: white, right panel: green) and stained for the mitochondrial protein TOM20 (middle panel: white, right panel: magenta) treated with 10 μM CCCP for 6 h. Scale bar = 10 μm. D) Quantification of EGFP-LC3 puncta colocalized with mitochondria in WT and VPS35D620N (clone 1 and 2) cells treated with 10 μM CCCP. Each dot represents one cell. Red lines show the median amount of EGFP-LC3 on mitochondria per cell line. Data analyzed using one-way ANOVA. **** $p < 0.001$

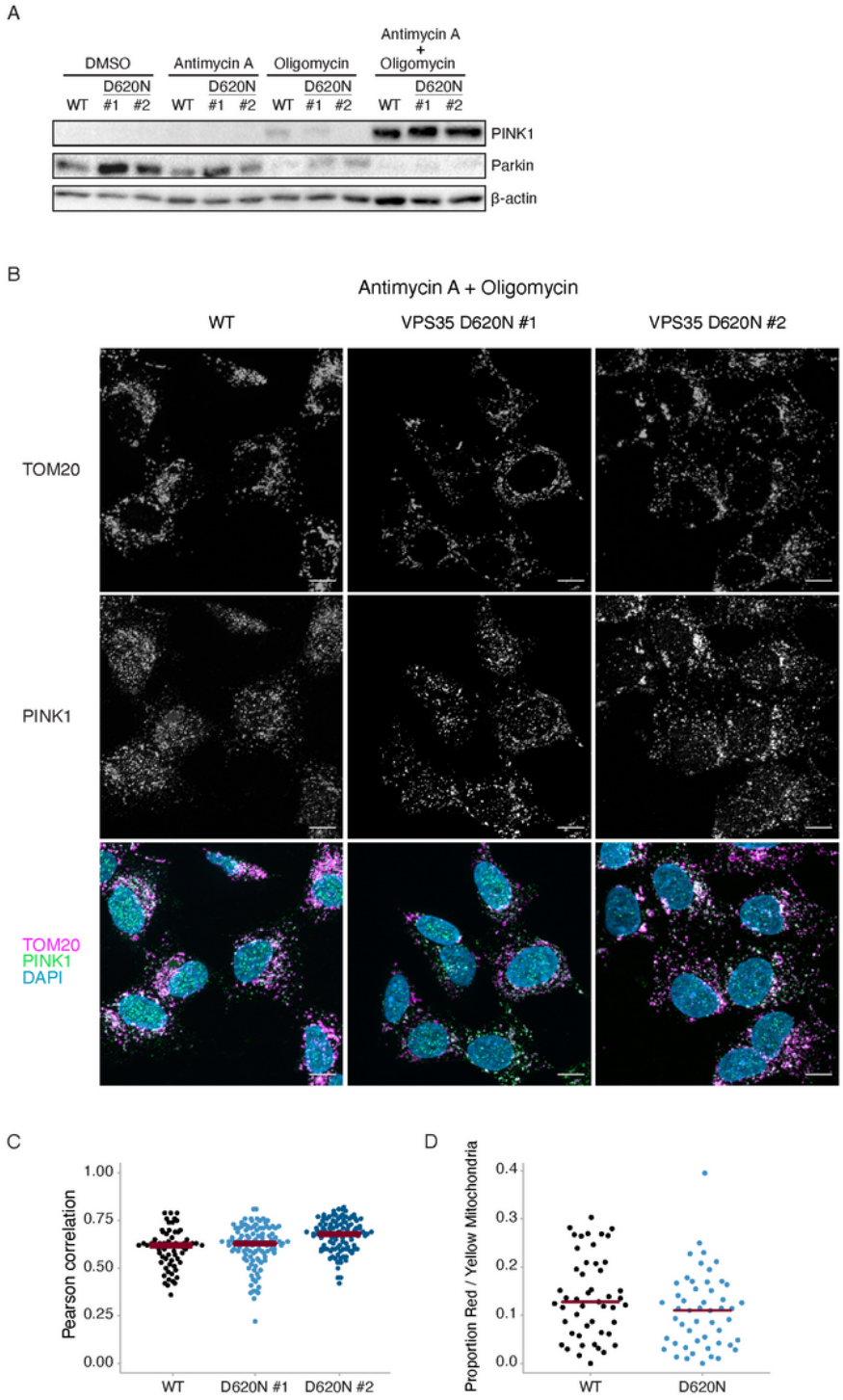

Figure 5

PINK1 accumulation is unaltered in VPS35D620N cells as result of depolarization via antimycin A and oligomycin. A) Representative immunoblots of protein extracts from WT and VPS35D620N (clone 1 and clone 2) cells treated with DMSO, 1 μM antimycin A, 1 μM oligomycin, or a combination of both drugs for 24 h. Blots were stained with PINK1, Parkin and β-actin (total protein loading control) antibodies. B) Representative fluorescence images of WT or VPS35D620N (clone 1 and 2) cells treated with 1 μM

antimycin A and 1 μM oligomycin. Upper panels show endogenous TOM20 staining. Middle panels show endogenous PINK1 staining. Lower panels show overlay image of TOM20 (magenta), PINK1 (green) and DAPI staining for nuclei (blue). Scale bar, 10 μm. C) Quantification of co-localization of endogenous TOM20 and PINK1 in WT and VPS35D620N (clone 1 and 2) cells treated with 1 μM antimycin A and 1 μM oligomycin, as shown in (B). Each dot represents the Pearson coefficient calculated for one cell. Red lines show the median Pearson coefficient per cell line. Statistical analysis was performed using a Kruskal-Wallis test followed by a pairwise Mann-Whitney U-test with Benjamini-Hochberg multiple testing correction. D) Quantification of yellow and red particles in WT and VPS35 D620N cells that stably express COX8-EGFP-mCherry treated with DMSO or with 1 μM antimycin A and 1 μM oligomycin for 24 h. Each dot represents the proportion of total yellow and red particles for one cell. Red lines show the median proportion per cell line per condition. Statistical analysis was performed using a beta regression.

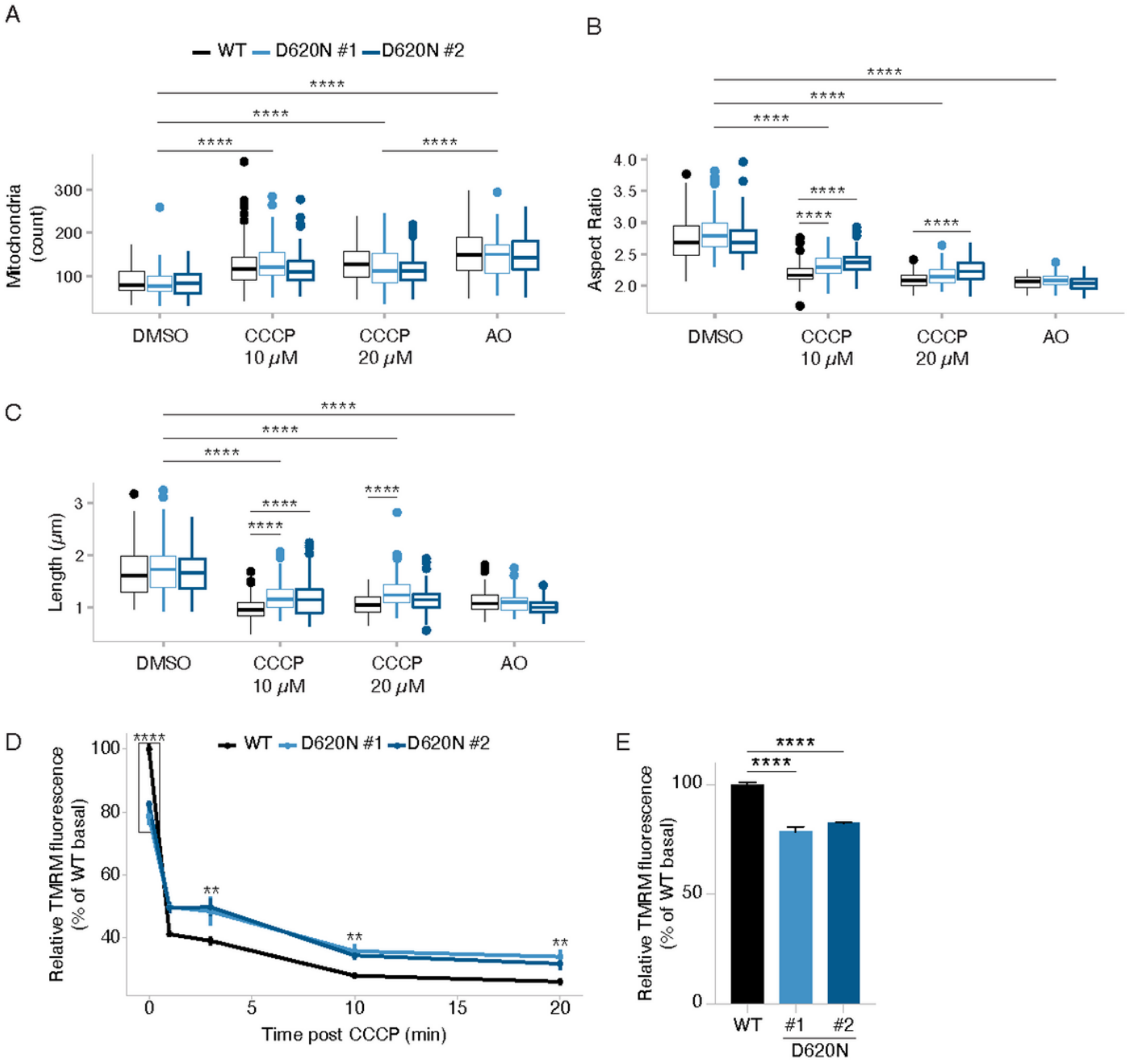

Figure 6

VPS35D620N cells are less susceptible to CCCP-induced mitochondrial depolarization. A-C) Quantification of mitochondrial morphology represented by number of mitochondria (A), aspect ratio (B) and length (C) as determined in TOM20-stained WT and VPS35D620N (clone 1 and 2) cells treated with DMSO, 10 μM CCCP, 20 μM CCCP or 1 μM antimycin A and 1 μM oligomycin for 24 h. D) Measurements of mitochondrial membrane potential by TMRM fluorescence of WT and VPS35D620N (clone 1 and 2) cells. TMRM fluorescence was measured at basal level and at 1, 3, 10 and 20 minutes after treatment

with 10 μM CCCP. E) Basal TMRM levels from boxed area highlighted in (D). Statistical analyses were performed using two-way ANOVA. *** p < 0.005, **** p < 0.001

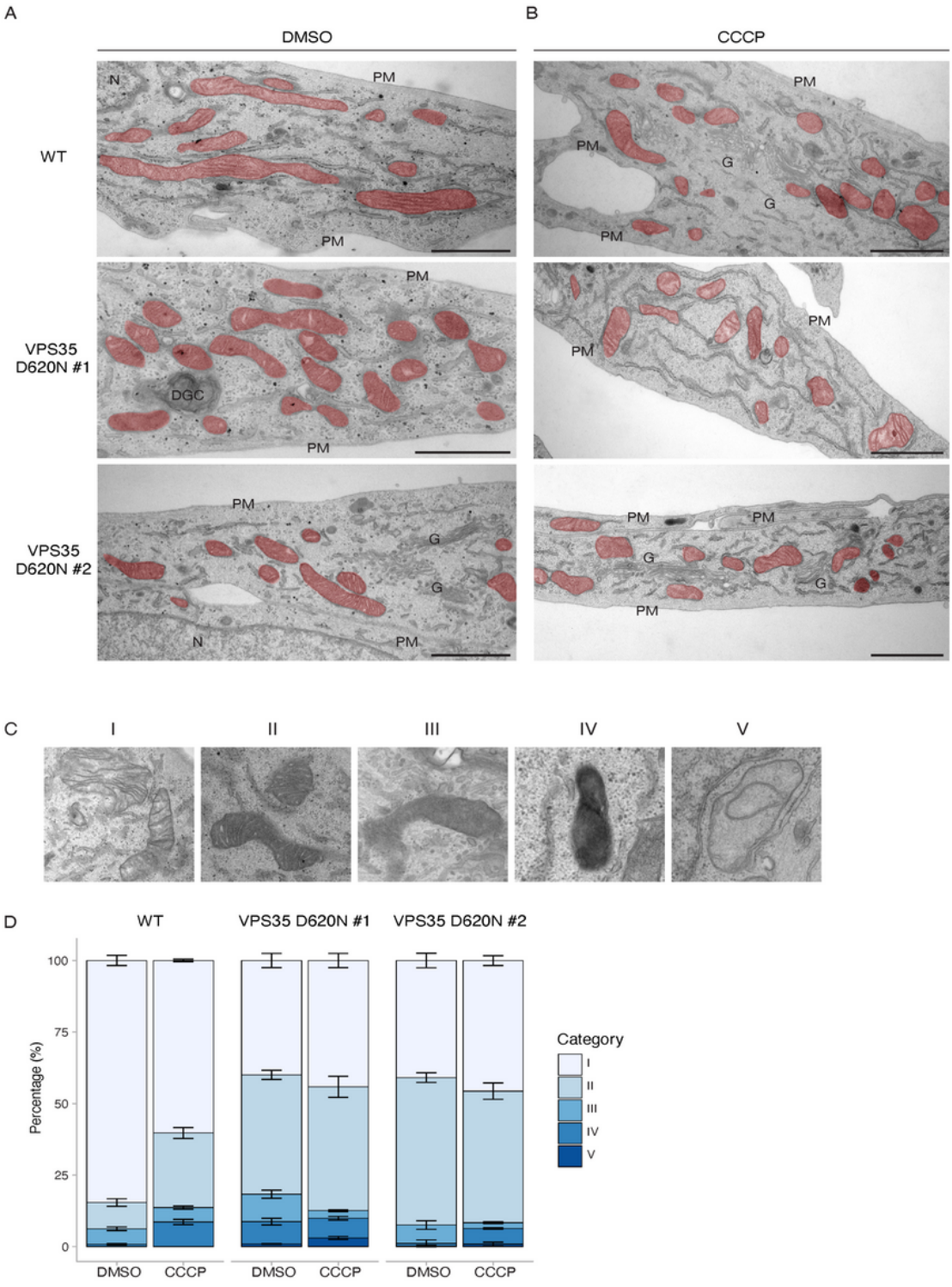

Figure 7

Mitochondria of VPS35D620N cells appear damaged under basal conditions and do not respond to CCCP. A-B) Representative TEM micrographs of WT and VPS35D620N (clone 1 and 2) cells treated with DMSO (A) or 10 μM CCCP for 6 h (B). Mitochondria are highlighted in red. DGC, degradative

compartment; G, Golgi apparatus; PM, plasma membrane. Scale bar, 1 µm. C) Representative examples of the mitochondria categories I – V. D) Quantification of the mitochondrial profile of WT or VPS35D620N (clone 1 and 2) cells treated with DMSO or 10 µM CCCP for 6 h.

Supplementary Files

This is a list of supplementary files associated with this preprint. Click to download.

- SupplementalFigure1.pdf
- SupplementaryTable1.xlsx